

Effect of C and Mn Variations Upon the Solidification Mode and Surface Cracking Susceptibility of Peritectic Steels

Eddy ALFARO LÓPEZ,¹⁾ Martín HERRERA TREJO,¹⁾ José Jorge RUÍZ MONDRAGÓN,¹⁾ Manuel de Jesús CASTRO ROMÁN¹⁾ and Hugo SOLÍS TOVAR²⁾

1) CINVESTAV-IPN, Unidad Saltillo, Carr. Saltillo-Mty Km. 13 Ramos Arizpe, Coah. México. E-mail: eddy.alfaro@cinvestav.edu.mx, martin.herrera@cinvestav.edu.mx, jorge.ruiz@cinvestav.edu.com.mx, manuel.castro@cinvestav.edu.mx

2) Ternium de México, S.A. de C.V., Ave. Cd. de los Angeles Ote. No. 325, Col. Garza Cantú, C.P. 66452, Col. San Nicolás de los Garza, Nuevo León, México. E-mail: sirhsy@sidor.com

(Received on December 19, 2008; accepted on February 23, 2009)

This work studies the effect of chemical composition, C and Mn contents, and cooling rate on both the solidification mode and the evolution of phases during the solidification of three steels; two of hypo-peritectic and one of hyper-peritectic composition. Furthermore, the cracking susceptibility associated to both the differences in mechanical behavior of δ and γ phases, and contraction during solidification, was inferred.

Slight variation of C or Mn, in the order of 0.04%, promoted significant changes in the evolution of phases during solidification. It was observed that for the hypo-peritectic steel closer to the peritectic point, the Mn microsegregation observed for high cooling rates promoted at the end of solidification a hyper-peritectic solidification mode. On the other hand, independently of the solidification mode and chemical composition of the studied steels, the differences in the mechanical behavior of δ and γ phases led to a cracking susceptibility in two solid fraction zones.

Furthermore, for the steel exhibiting hypo-peritectic solidification mode the peritectic transformation occurred at higher solid fraction compared with the steels showing hyper-peritectic solidification mode. Therefore, the remaining liquid ability to feed the contraction in the solid-liquid shell associated to the peritectic transformation resulted adversely affected. Hence, the cracking susceptibility observed in the hypo-peritectic steel is not only generated by differences in the mechanical behavior of δ and γ phases, but also by the liquid inability to compensate the contraction associated to the peritectic transformation.

KEY WORDS: solidification mode; peritectic transformation; cooling conditions; cracking susceptibility.

I. Introduction

Continuously cast carbon steel slabs frequently exhibit surface cracking susceptibility, which is associated with their solidification mode. It is accepted that surface cracking susceptibility is promoted by volumetric contraction associated with peritectic solidification, liquid (L) + $\delta_{(bcc)}$ \rightarrow $\gamma_{(fcc)}$, which begins in the mold of the continuous casting machine.^{1–7)}

Mn is a chemical element found in carbon steel slabs, with typical content ranging between 0.5 and 1.5% (weight percent). **Figure 1** shows two calculated pseudo-binary equilibrium Fe–C–XMn diagrams for steels with different Mn content, in which X is either 0.77 or 1.17%. In this figure, it is observed that an increase in Mn content shifts the peritectic “point” to lower carbon contents and lower temperature values. For illustration purposes of Mn effect, in Fig. 1, C content of 0.14% is indicated by a vertical line, thus, for 1.17% of Mn the solidification mode is hyper-peritectic, *i.e.* after the ending of the peritectic transformation the γ phase is formed from the remaining liquid, in contrast, for the steel with 0.77% of Mn, the solidification mode is hypo-peritectic, *i.e.* after the peritectic transfor-

tion, the growth of the γ phase continues at the expense of the δ phase. On the other hand, solute microsegregation during solidification alters the local equilibrium conditions at the solid-liquid interface and can modify the phase evolution during solidification.^{8,9)} It is thought that a so-called hypo-peritectic steel can eventually solidify like hyper-peritectic steel because of microsegregation effect, which is promoted by increasing cooling rate.

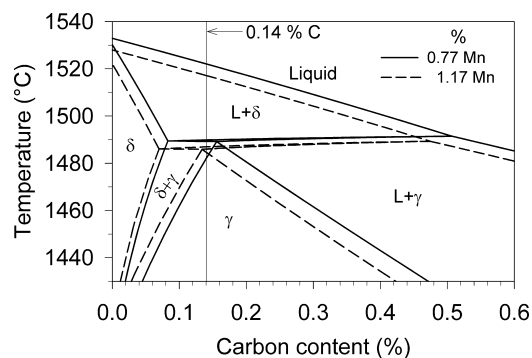


Fig. 1. Comparison between equilibrium Fe–C–XMn pseudo-binary diagrams calculated for two peritectic steels.

In this context, control of the surface cracking susceptibility of peritectic steels requires knowledge about both the evolution of phases during solidification and the description of the mechanical behavior of the solidified shell. The experimental description of phase evolution during solidification in the continuous casting process is difficult due to the high temperatures and high cooling rates involved. Thus, mathematical modeling is frequently used, integrating several approaches with different degrees of complexity which have been proposed to describe not only the solid state diffusion but also the solute segregation in the remaining liquid involved during peritectic solidification. Nowadays, DICTRA software (Diffusion Controlled Transformations)¹⁰⁾ allows us to simulate diffusive transformations with moving boundaries. It integrates thermodynamic and kinetic databases to solve one-dimensional diffusion equations for multicomponent systems, using the Thermocalc¹¹⁾ software to calculate local equilibrium at the involved interfaces.

In order to study in depth the effect of chemical composition and cooling rate on both the solidification mode and surface cracking susceptibility of peritectic carbon steels, this study combines a thermal analysis technique with mathematical simulation of solidification. Thus, the solidification behavior of a hyper-peritectic steel was compared to that of two hypo-peritectic steels. The chemical composition of the hyper-peritectic steel was considered as reference, and the first and second hypo-peritectic steels were obtained by reducing C and Mn content, respectively. The phase evolution during solidification is described for different cooling rates, which are similar to those reported for conventional slabs.¹²⁾ Furthermore, the mechanical behavior and thermal contraction of the solidified shell were evaluated as a function of the solid fraction evolution.

2. Experimental Procedure

In the first stage of this study, a thermal analysis technique was applied in solidification experiments on three peritectic carbon steels in order to obtain thermal and microstructural information under three different continuous cooling conditions. In the second stage, the experimental information was couple to the software in order to obtain phase evolution during solidification. Subsequently, mechanical properties and thermal contraction developed in each steel during solidification were calculated.

Three steels with different content of C and Mn were studied and they were named HC-HMn, HC-LMn and LC-HMn, where H and L mean “High” and “Low” respectively, e.g. HC-HMn means high C and high Mn steel. These steels correspond to one hyper-peritectic and two hypo-peritectic steels, for which chemical composition is specified in **Table 1**.

Table 1. Chemical composition of steels (mass%).

Steel	Code	C	Mn	Si	S	P	Cr	Ni	Al	Cu
Hyper-peritectic	HC-HMn	0.14	1.17	0.25	0.005	0.016	0.02	0.015	0.023	0.062
Hypo-peritectic	HC-LMn	0.14	0.77	0.15	0.008	0.081	0.026	0.085	0.042	0.082
Hypo-peritectic	LC-HMn	0.10	1.17	0.25	0.005	0.017	0.02	0.015	0.023	0.064

2.1. Thermal Analysis

Since the experimental method for thermal analysis has already been described in a previous paper published by Ruiz *et al.*,⁹⁾ no details will be provided in this paper about this technique.

In order to estimate the solidification time (time elapsed in the solid–liquid region) and the cooling rate for each thermal analysis experiment, the determination of liquidus (T_l) and solidus (T_s) temperatures from the cooling curves was necessary. Thus, the cooling curve obtained for each steel at the lowest cooling rate, which is assumed to be close to the equilibrium condition, was initially considered. Then T_l and T_s , using equilibrium pseudo-binary diagrams, were associated with peaks in the first and second derivatives of the cooling curve. After determining the peaks associated with the transformation temperatures, these peaks were identified for all cooling conditions for each steel.

2.2. Simulation of Solidification Process

Initial chemical composition, cooling curve and control volume characteristics were fed into the software¹⁰⁾ for each simulation. Initial chemical composition considered C, Mn, and Si, as specified in Table 1. In the same table the hypo-peritectic or hyper-peritectic steel grade is also indicated. The control volume was chosen considering a dendritic columnar structure; the secondary dendrite arm spacing (λ) was selected as the characteristic longitude at the microsegregation scale, as originally proposed by Broody and Flemings.¹³⁾

Assuming regular spacing for the secondary dendrite arms as well as symmetrical properties between them, the control volume is half λ . The λ value associated with each cooling condition was calculated using Eq. (1), reported for steels solidified at different cooling rates:

$$\lambda = 26.1 \times t_s^{0.38} \dots\dots\dots(1)$$

where λ is expressed in μm and t_s in s.⁵⁾ The t_s values were obtained from the experimental cooling curves. The control volume has been illustrated in a previous paper,⁹⁾ in which the initial thickness value for δ and γ phase in each simulation was $\lambda/20$. The kind of grid used was double geometrical, dividing the region into two halves and generating a separate geometric grid (300) node in each half, thus allowing contact between the two phases, with one of them acting as interface for the other one, keeping a uniform inter-spacing of the grid for a closed system.¹⁰⁾ The simulation was conducted employing the kinetic MOB2 and thermodynamic SSOL databases.

2.3. Tensile Properties

Calculation of the mechanical properties evolution of the solidified steel shell was carried out using the following

equations reported by Mizukami *et al.*⁸⁾

$$\sigma_{\delta}^{L/S} = 6.0 \times (f_s - 0.8) \times f_{\delta} \dots \dots \dots (2)$$

$$\sigma_{\gamma}^{L/S} = 33.5 \times (f_s - 0.8) \times f_{\gamma} \dots \dots \dots (3)$$

$$\varepsilon_{\delta}^{L/S} = 6.5 \times (f_s - 0.8) \times f_{\delta} \dots \dots \dots (4)$$

$$\varepsilon_{\gamma}^{L/S} = 6.5 \times (f_s - 0.8) \times f_{\gamma} \dots \dots \dots (5)$$

where f_i is the fraction of phase i ; i can be s , δ or γ phases; $\sigma_i^{L/S}$ is the tensile strength generated in phase i , expressed in MPa; $\varepsilon_i^{L/S}$ is the elongation of phase i , expressed in %. These equations have been validated for carbon and alloyed steels and solid fractions between 0.8 and 1.0.¹⁴⁾

2.4. Contraction

The thermal contraction associated with the phase growth during solidification was calculated using the mathematical expression given by Jablonka *et al.*¹⁵⁾:

$$\varepsilon^{th}(T) = \sqrt[3]{\frac{\rho(T_{ref})}{\rho(T)}} - 1 \dots \dots \dots (6)$$

where $\varepsilon^{th}(T)$ is the thermal contraction at temperature T , $\rho(T_{ref})$ and $\rho(T)$ are the densities at the reference temperature T_{ref} and at temperature T , respectively. In the case of peritectic transformation in which several phases are involved, the average density at temperature T can be calculated with the following expression:

$$\rho(T) = \frac{1}{\sum_{n=1}^p \left[\frac{f_n(T)}{\rho_n(T)} \right]} \dots \dots \dots (7)$$

where $f_n(T)$ and $\rho_n(T)$ are phase fraction and density, respectively, for each n phase coexisting at temperature T . The phase density can be obtained using the equation suggested by Miettinen,¹⁶⁾ as a function of both temperature and chemical composition.

3. Results and Discussion

3.1. Thermal Analysis

Figures 2(a)–2(c) show the cooling curves obtained for the three studied steels at each cooling condition. The cooling rate values described in Fig. 2 were the result of the averaging of fractions, *i.e.* the lowest cooling rates were between 0.29–0.33°C/s, while intermediate cooling rates were between 2.8–3.3°C/s, and the highest cooling rates were between 9.8–10.0°C/s. Thus, practically three cooling rate values were obtained: 0.3, 3 and 10°C/s.

Figures 3(a) and 3(b) show the Fe–C pseudo-binary equilibrium diagrams calculated for each steel. C content and equilibrium transformation temperatures are indicated with a vertical line in each figure. Figure 3(a) shows the diagram belonging to HC-LMn hypo-peritectic steel, which has the lowest Mn content. Figure 3(b) shows the diagram belonging to hypo-peritectic and hyper-peritectic steels, LC-HMn and HC-HMn respectively, whose only difference is their C content.

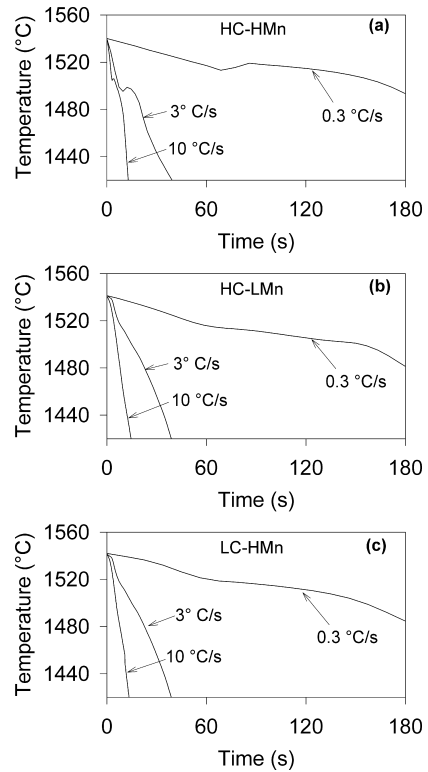


Fig. 2. Continuous cooling curves.

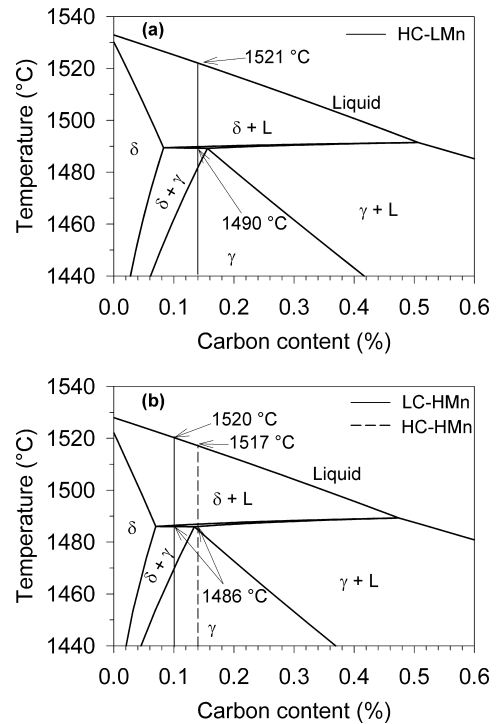


Fig. 3. Fe–C equilibrium pseudo-binary diagrams.

In order to illustrate the thermal analysis conducted, the HC-LMn steel was selected, shown in Fig. 3(a). From this figure, the solidification starting and peritectic transformation temperatures were obtained as 1521 and 1490°C, respectively. Furthermore, Figs. 4(a) and 4(b) show the first and second derivatives, respectively, of the cooling curve obtained for the HC-LMn steel at the lowest cooling rate, which is assumed to be close to the equilibrium conditions. In these figures, it is observed that the temperatures pre-

dicted using the equilibrium diagram, Fig. 3(a), can be associated with peaks appearing in the first and second derivatives of the cooling curve. The second derivative of the cooling curve exhibited a peak after which no significant thermal fluctuations were observed, except for the continuous cooling of the sample. This peak was associated with the end of solidification and it corresponded to 1472°C. In this way, it was possible to estimate the solidification time, t_s , and cooling rate. The behavior shown in Figs. 4(a) and 4(b) was systematically observed for all cooling rates in each steel. The determined temperatures and the estimated parameters t_s , λ and cooling rate are given in **Table 2**.

3.2. Simulation

Figures 5(a)–5(c) show the phase evolution at values of solid fraction higher than 0.8, for which it is accepted that the solidified shell begins to develop its mechanical properties.⁸⁾ For the HC-HMn and HC-LMn steels, Figs. 5(a) and 5(b), it is observed that the phase evolution during solidification was independent of cooling rate. In contrast, for the

LC-HMn steel the effect of the cooling rate is appreciable after the peritectic transformation started. For the three studied steels the fraction of δ phase increased up to the point where the peritectic reaction is reached. From this point, γ phase grew at the expense of δ phase and liquid.⁴⁾ Moreover, it is observed that the peritectic reaction occurred at different solid fraction values depending on the steel. For the HC-HMn and HC-LMn steels, Figs. 5(a) and 5(b) respectively, δ phase reached its highest solid fraction value at 0.81 and 0.83 respectively, whereas for the case of the LC-HMn steel, Fig. 5(c) shows that δ phase reached its highest solid fraction value at 0.9. This difference is associated to the C effect on the solidification mode, *i.e.* the LC-

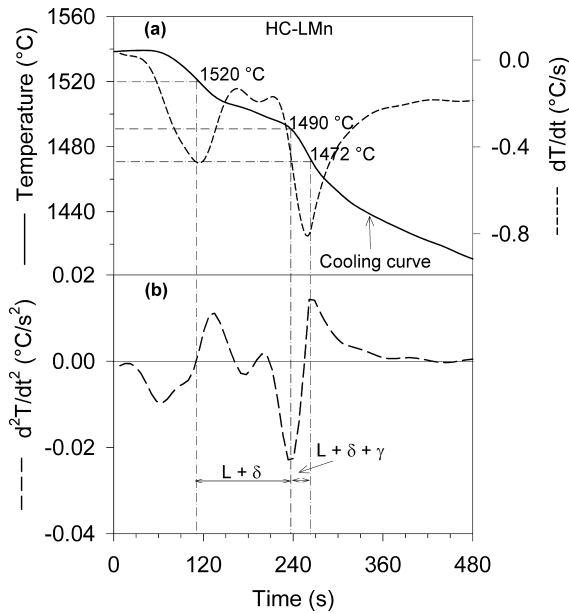


Fig. 4. Thermal analysis of HC-LMn steel carried out at a cooling rate of 0.3°C/s.

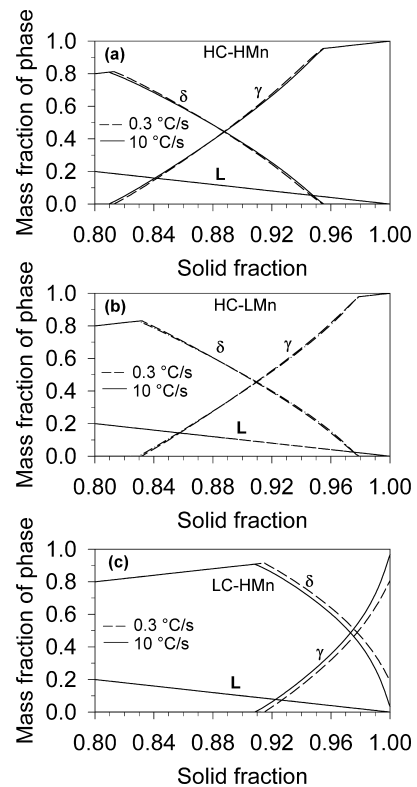


Fig. 5. Evolution of mass fraction of phases as a function of solid fraction for two cooling rates in (a) HC-HMn, (b) HC-LMn and (c) LC-HMn steels.

Table 2. Values obtained from the continuous cooling curves generated by thermal analysis.

Steel	Starting solidification temperature (°C)	Ending solidification temperature (°C)	Solidification time, t_s (s)	Secondary dendrite arm, λ (μm)	Cooling rate (°C/s)
HC-HMn	1519	1480	120	161	0.33
	1519	1464	19	80	2.9
HC-LMn	1519	1430	9	60	9.89
	1520	1472	150	175	0.32
	1524	1467	20	82	2.85
LC-HMn	1516	1426	9	60	10
	1525	1470	168	183	0.33
	1521	1461	21	83	2.86
	1519	1430	9	60	9.89

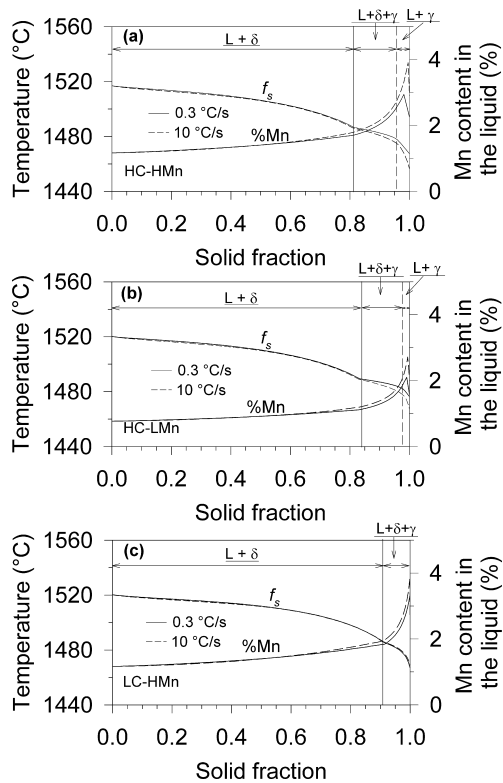


Fig. 6. Variation of Mn content in the remaining liquid as a function of solid fraction for two cooling rates in (a) HC-HMn, (b) HC-LMn and (c) LC-HMn steels.

HMn steel has the lowest C content, and therefore its solid/liquid ratio at the peritectic reaction temperature is higher than that for the other steels. Moreover, it is seen that HC-HMn and HC-LMn steels, Figs. 5(a) and 5(b) respectively, are characterized by a hyper-peritectic solidification mode whereas the LC-HMn steel exhibited a hypo-peritectic solidification mode. It is noteworthy that the so-called hypo-peritectic HC-LMn steel, Table 1, exhibited a hyper-peritectic solidification mode, according to the evolution of phases shown in Fig. 5(b); this change of solidification mode is associated with Mn microsegregation during solidification.

The mass content of the alloying elements in the remaining liquid as a function of the solid fraction growth was evaluated. For illustration purposes, Figs. 6(a)–6(c) show the results obtained for each steel at two cooling rates for the case of Mn, which had the highest microsegregation level compared to the other elements. In these figures, the solid fraction at which the peritectic transformation begins is indicated by a vertical solid line, whereas the end of this transformation is indicated by a discontinue line. It is observed that Mn microsegregation is highest at the end of solidification; also, this microsegregation is promoted at the end of solidification by an increase in the cooling rate. On the one hand, in a comparison between hyper-peritectic HC-HMn and hypo-peritectic HC-LMn steels, Figs. 6(a) and 6(b) respectively, in which the difference in chemical composition is only 0.4% Mn, *i.e.* the Mn content is decreased from 1.17 for the HC-HMn steel to 0.77% for the HC-LMn steel, the solid fraction value at which the $\delta \rightarrow \gamma$ transformation occurs is displaced from 0.81 to 0.84. This means that for the HC-HMn steel, there is 3.5% more liquid phase to

feed the contraction generated during solidification. On the other hand, in a comparison between hyper-peritectic HC-HMn and hypo-peritectic LC-HMn steels, Figs. 6(a) and 6(c) respectively, in which the Mn content is 1.17% and the C content is decreased from 0.14 for the HC-HMn steel to 0.10% for the LC-HMn steel, the solid fraction value at which the $\delta \rightarrow \gamma$ transformation occurs is displaced from 0.81 to 0.91. This indicates that there is 10% more liquid phase to feed the contraction generated during solidification in the HC-HMn steel. Thus, assuming that it is desirable that the peritectic transformation occurs at sufficiently low solid fractions in order to promote enough liquid phase to compensate the contraction produced during solidification,^{17–20} Figs. 5 and 6 show that an increase in C content shifts more extensively the peritectic transformation to lower values of solid fraction compared with the effect of Mn. These figures also suggest that the solidification mode of carbon steels can be positively influenced by increasing Mn content given that this element promotes the hyper-peritectic solidification mode. Thus, it is observed that a slight variation in the chemical composition, 0.4% of Mn or 0.04% of C, promotes changes in the proportion of phases during solidification. This means that the mechanical behavior of the solidified shell formed in the continuous casting mold can be altered by modifying the steel chemical composition.

3.3. Tensile Strength and Elongation during Solidification

According to the peritectic transformation mechanism in which δ and γ phases are in contact with each other, it is assumed that a difference in the mechanical behavior of the phases at high temperatures can induce strain in their interfaces and consequently promote the generation of cracks.^{8,14} Equations (2)–(5) were used to calculate tensile strength and elongation for the δ and γ phases as a function of the solid fraction evolution. Considering that the evolution of phases, tensile strength and elongation were practically independent of the cooling rate, Figs. 7–9 show the results obtained for only one cooling rate, 10°C/s, which is a similar value to those found in regions close to the slab surface.¹² The dark areas show the ranges of solid fraction values in which strain could be induced in the δ/γ interface.

Figures 7(a), 8(a) and 9(a) show the mass fraction evolution of δ and γ phases during solidification as a function of solid fraction for HC-HMn, HC-LMn and LC-HMn steels respectively. It can be seen that in the case of the HC-HMn steel, Fig. 7(a), the fraction of δ phase increased up to a solid fraction value near 0.81, after which γ phase began to grow. For the HC-LMn steel, Fig. 8(a), γ phase began to appear at a solid fraction of 0.83, whereas for the LC-HMn steel, Fig. 9(a), γ phase was formed up to a solid fraction value of 0.91. For solid fraction values higher than 0.81, the HC-HMn steel shows that the δ phase fraction decreased becoming equal to that of γ phase at a solid fraction of 0.89, whereas for the HC-LMn and LC-HMn steels the same behavior occurred at solid fraction values of 0.91 and 0.975 respectively. Later, in HC-HMn and HC-LMn steels, δ phase disappeared at solid fraction values of 0.955 and 0.98 respectively, and subsequently an additional amount of γ phase was formed from the remaining liquid. In contrast,

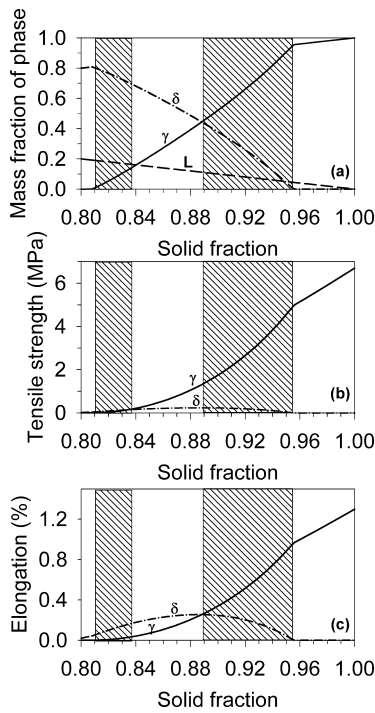


Fig. 7. Relationship between (a) mass fraction of phase, (b) tensile strength, (c) elongation and solid fraction for HC-HMn steel sample.

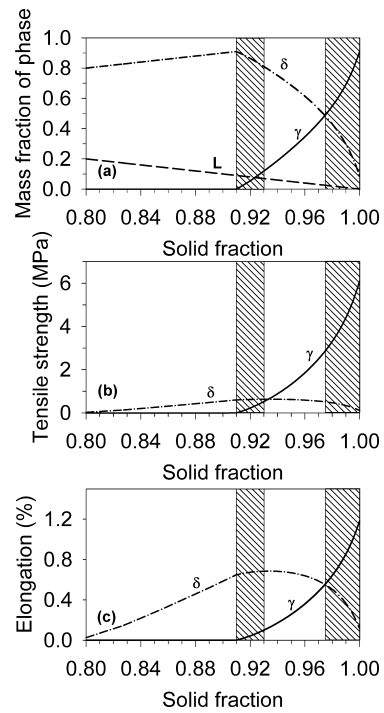


Fig. 9. Relationship between (a) mass fraction of phase, (b) tensile strength, (c) elongation and solid fraction for HC-LMn steel sample.

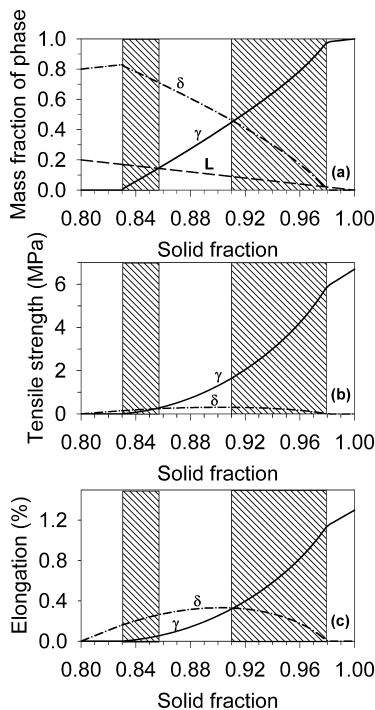


Fig. 8. Relationship between (a) mass fraction of phase, (b) tensile strength, (c) elongation and solid fraction for HC-LMn steel sample.

for the LC-HMn steel, both δ and γ phases are still present at the end of solidification.

Figures 7(b), 8(b), 9(b) and 7(c), 8(c), 9(c) show the variation of tensile strength and elongation respectively for the δ and γ phases, with respect to solid fraction for the three studied steels. A similar behavior was observed for the three steels, which was characterized by the presence of two zones in which strain at the δ/γ interface is generated and

therefore cracking susceptibility arises. The first zone is associated to a range of solid fraction whose lower value corresponds to the beginning of the peritectic transformation. In this zone γ phase shows the lowest values of tensile strength and elongation, indicating that in this range of solid fractions the strain was generated in the γ phase. For this zone, the solid fraction ranges 0.81–0.84, 0.83–0.857 and 0.91–0.93 were associated to the HC-HMn, HC-LMn and LC-HMn steels respectively. After the first zone and until the fractions of δ and γ phases become equal, δ phase showed lower tensile strength and higher elongation compared with γ phase. Consequently, in this solid fraction range strain was not generated in any phase. The second zone showing cracking susceptibility starts where the fractions of δ and γ phases are the same and it continues until the peritectic transformation finishes. In this solid fraction range, γ phase exhibited higher tensile strength and higher elongation values than δ phase, indicating that the strain is generated in the δ phase. Furthermore, the solid fraction ranges for this zone were 0.885–0.955, 0.91–0.98 and 0.975–1.0 for HC-HMn, HC-LMn and LC-HMn steels, respectively.

The mechanical behavior illustrated in Figs. 7–9 for the three steels studied, agrees qualitatively with that observed by Ruiz *et al.*⁹⁾ in a hypo-peritectic steel containing 0.13% C and 1.15% Mn, where zones of cracking susceptibility were found in two solid fraction ranges, 0.85–0.87 and 0.92–0.98. Also, it is noteworthy that the hypo-peritectic steel studied by Ruiz *et al.*⁹⁾ exhibited a hyper-peritectic solidification mode, as observed in the present work for the HC-LMn hypo-peritectic steel. Moreover, there was also good concordance with the results obtained by Mizukami *et al.*⁸⁾ in a carbon steel containing 0.14% C and in a low alloy steel with 0.11% C, 0.5% Mn and 0.1% Si, whose zones of

cracking susceptibility were found within solid fraction ranges of 0.88–0.92 and 0.98–1.0 for the former steel, and 0.94–0.965 and 0.99–0.995 for the second one. For the case of the latter steel, Mizukami⁸⁾ suggested that the end of solidification was characterized by formation of γ phase from the liquid phase, as observed in HC-HMn and HC-LMn steels in the present work. However, in the case of the LC-HMn steel, which contains 0.10% C and 1.17% Mn, it was observed that the $\delta \rightarrow \gamma$ transformation continued in the solid state.

3.4. Contraction

In order to illustrate the effect of slight variations of C and Mn in chemical composition of peritectic steels, on the contraction levels generated during solidification at different cooling rates, Figs. 10(a)–10(c) show contraction levels calculated using Eqs. (6) and (7) as a function of solid fraction for each studied steel. The previously obtained zones of cracking susceptibility and the solid fraction of 0.9 associated with the “Liquid Impenetrable Temperature” (LIT)^{17–20)} are shown in each figure. In all cases, the contraction levels were independent of cooling rate. The HC-HMn and HC-LMn steels, Figs. 10(a) and 10(b), characterized by a hyper-peritectic solidification mode exhibited a slight expansion at solid fraction values of 0.955 and 0.98, respectively. This behavior was associated to the formation of γ phase from a highly saturated liquid at the end of solidification, shown in Fig. 6. Recently, Ruiz *et al.*⁹⁾ observed the same behavior for a steel exhibiting hyper-peritectic solidification mode. Moreover, the contraction levels observed in these steels are comparable to that reported by Miettinen¹⁶⁾ for a hyper-peritectic steel containing 0.162% C and 0.5% Mn. On the other hand, Fig. 10(c) shows the behavior observed for the hypo-peritectic LC-HMn steel, which exhibited a progressive contraction. The contraction level at the end of solidification was similar to those observed for HC-HMn and HC-LMn steels with hyper-peritectic solidification mode.

Considering the criterion proposed by Clyne *et al.*,²⁰⁾ which relates the incidence of cracking to solid fractions higher than 0.9 where the remaining liquid is unable to feed the contraction, it is thought that a cause of the cracking susceptibility depends on the solid fraction range within which the peritectic transformation takes place, *i.e.* whether peritectic transformation occurs when the contraction can be compensated by the liquid phase ($f_s < 0.9$), or whether it occurs when no liquid feeds the contraction generated ($f_s > 0.9 = \text{LIT}_s$).^{17–20)} Thus, it is expected that the highest cracking susceptibility is associated to the hypo-peritectic LC-HMn steel for which the peritectic transformation starts at a solid fraction of 0.91 and, therefore, the contraction generated by the peritectic transformation cannot be compensated by the liquid phase. This is confirmed by the accumulated thermal contraction within the solid fraction range of 0.9–1.0, with values of 0.00226, 0.00237 and 0.0034 were associated to the HC-HMn, HC-LMn and LC-HMn steels respectively, Figs. 10(a)–10(c). Consequently, the accumulated contraction observed for the hypo-peritectic LC-HMn steel was approximately 30% higher than those associated with the HC-HMn and HC-LMn steels which exhibited hyper-peritectic solidification mode.

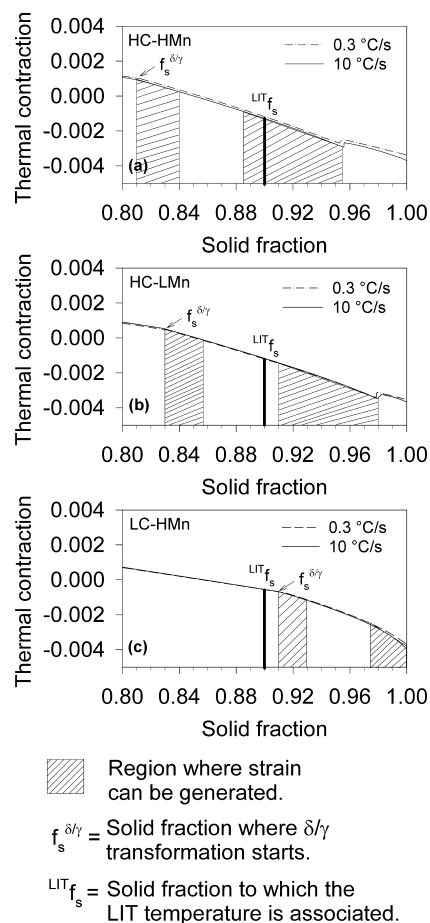


Fig. 10. Relationship between thermal contraction and solid fraction for two cooling rates in each steel.

Furthermore, for the hyper-peritectic HC-HMn steel, Fig. 10(a), the peritectic transformation began at a solid fraction of 0.81 and only a portion of the second zone of cracking susceptibility, associated to strain generation at the δ/γ interface, was located at solid fraction values higher than 0.9. Hence, in the solid fraction range of 0.9–0.955, the differences in the mechanical properties of δ and γ phases and the thermal contraction represent causes of the cracking susceptibility. Similar behavior was observed for the HC-LMn steel, which exhibited hyper-peritectic solidification mode, shown in Fig. 10(b), however, in this case the causes of the cracking susceptibility were observed in the range of solid fraction of 0.91–0.98. Moreover, for the hypo-peritectic LC-HMn steel, Fig. 10(c), the two solid fraction zones (0.91–0.93 and 0.97–1.0) of crack susceptibility associated to the strain at the δ/γ interface are included in the solid fraction range within which the contraction cannot be fed by the remaining liquid. Therefore, it is thought that the hypo-peritectic steel will be more sensitive to exhibit cracking susceptibility.

4. Conclusions

From the description of the evolution of phases during solidification and the mechanical behavior evaluated as a function of solid fraction for three peritectic steels, the following conclusions were drawn:

(1) For the studied hypo-peritectic steels, a slight variation of C and/or Mn contents affects the proportion of

phases during solidification. The variation in the C content has a larger influence than that of Mn on the evolution of phases, however, the Mn microsegregation generated at high cooling rate can promote a change in the solidification mode from hypo to hyper-peritectic.

(2) The proportion of phases exhibited during solidification affects the mechanical behavior of the solidified shell. Independently of the cooling rate and the steel chemical composition, the cracking susceptibility associated with differences in the mechanical behavior of δ and γ phases, occurred into two solid fraction zones.

(3) The cracking susceptibility exhibited by peritectic steels depends also on the solid fraction value at which the peritectic transformation takes place. *i.e.* if the remaining liquid is able to feed the accumulated contraction generated by the peritectic transformation.

(4) The cracking susceptibility frequently observed in hypo-peritectic steels is then associated not only with differences in the mechanical behavior of δ and γ phases, but also with the liquid inability to compensate the contraction associated with the peritectic transformation.

REFERENCES

- 1) E. T. Turkdogan: Fundamentals of Steelmaking, The Institute of Materials, London, (1996), 104.
- 2) Y. M. Won, T. J. Yeo, D. J. Seol and K. H. Oh: *Metall. Mater. Trans. B*, **31B** (2000), 779.
- 3) J. Konishi, M. Militzer, J. K. Brimacombe and I. V. Samarasekera: *Metall. Mater. Trans. B*, **33B** (2002), 413.
- 4) D. M. Stefanescu: *ISIJ Int.*, **46** (2006), 786.
- 5) C. Cicutti and R. Boerl: *Steel Res. Int.*, **77** (2006), 194.
- 6) Y. M. Won, H. N. Han, T. J. Yeo and K. H. Oh: *ISIJ Int.*, **40** (2000), 129.
- 7) Y. M. Won and B. G. Thomas: *Metall. Mater. Trans. A*, **32A** (2001), 1755.
- 8) H. Mizukami, A. Yamanaka and T. Watanabe: *ISIJ Int.*, **42** (2002), 964.
- 9) J. Ruiz, M. Herrera, M. Castro and H. Solís: *ISIJ Int.*, **48** (2008), 454.
- 10) DICTRA Software, Tool for Simulation of Diffusional Transformations in Alloys, 24, Foundation of Computational Thermodynamics, Stockholm, Sweden, (2006).
- 11) A. Thermo-Calc Software AB. The Phase Diagram in multicomponent alloys, R, Foundation of Computational Thermodynamics, Stockholm, Sweden, (2006).
- 12) S. Louhenkilpi, J. Miettinen and L. Holappa: *ISIJ Int.*, **46** (2006), 914.
- 13) D. Brody and C. Flemings: *Trans. Metall. Soc. AIME*, **236** (1966), 615.
- 14) H. Mizukami, Y. Shirai and A. Yamanaka: *ISIJ Int.*, **46** (2006), 1040.
- 15) A. Jablonka, K. Harste and K. Schwerdtfeger: *Steel Res. Int.*, **62** (1991), 24.
- 16) J. Miettinen: *Scand. J. Metall.*, **22** (1993), 317.
- 17) K. H. Kim, T. J. Yeo, K. H. Oh and D. N. Lee: *ISIJ Int.*, **36** (1996), 284.
- 18) Y. M. Won, K. H. Kim, T. J. Yeo and K. H. Oh: *ISIJ Int.*, **38** (1998), 1093.
- 19) D. J. Seol, Y. M. Won, K. H. Oh, Y. C. Shin and C. H. Yim: *ISIJ Int.*, **40** (2000), 356.
- 20) T. W. Clyne, M. Wolf and W. Kurz: *Metall. Mater. Trans.*, **13B** (1982), 259.